Published in final edited form as:
J Biomech. 2012 August 9; 45(12): 2157–2163. doi:10.1016/j.jbiomech.2012.05.037.

Three-Dimensional Modular Control of Human Walking

Jessica L. Allen and **Richard R. Neptune**
Department of Mechanical Engineering, The University of Texas at Austin, TX

Abstract

Recent studies have suggested that complex muscle activity during walking may be controlled using a reduced neural control strategy organized around the co-excitation of multiple muscles, or modules. Previous computer simulation studies have shown that five modules satisfy the sagittal-plane biomechanical sub-tasks of 2D walking. The present study shows that a sixth module, which contributes primarily to mediolateral balance control and contralateral leg swing, is needed to satisfy the additional non-sagittal plane demands of 3D walking. Body support was provided by Module 1 (hip and knee extensors, hip abductors) in early stance and Module 2 (plantarflexors) in late stance. In early stance, forward propulsion was provided by Module 4 (hamstrings), but net braking occurred due to Modules 1 and 2. Forward propulsion was provided by Module 2 in late stance. Module 1 accelerated the body medially throughout stance, dominating the lateral acceleration in early stance provided by Modules 4 and 6 (adductor magnus) and in late stance by Module 2, except near toe-off. Modules 3 (ankle dorsiflexors, rectus femoris) and 5 (hip flexors and adductors except adductor magnus) accelerated the ipsilateral leg forward in early swing whereas Module 4 decelerated the ipsilateral leg prior to heel-strike. Finally, Modules 1, 4 and 6 accelerated the contralateral leg forward prior to and during contralateral swing. Since the modules were based on experimentally measured muscle activity, these results provide further evidence that a simple neural control strategy involving muscle activation modules organized around task-specific biomechanical functions may be used to control complex human movements.

Keywords

Forward dynamic simulation; Mediolateral balance control; Power transfer; Muscle synergies

Introduction

Previous studies suggest that non-impaired walking may be achieved using a reduced set of neural control elements or modules (e.g., Cappellini et al., 2006; Clark et al., 2010; Ivanenko et al., 2004). Recent 2D modeling and simulation studies examined whether these modules are structured to perform task-specific sagittal-plane biomechanical functions (i.e., body support, forward propulsion and leg swing) (McGowan et al., 2010; Neptune et al., 2009). In these studies, four modules identified from electromyography (EMG) activity in healthy

Please address correspondence to: Richard R. Neptune, Ph.D, Department of Mechanical Engineering, The University of Texas at Austin, 1 University Station C2200, Austin, TX 78712 USA, rneptune@mail.utexas.edu, Phone: (512) 471-0848, Fax: (512) 471-8727.

Conflict of interest statement
There is no conflict of interest regarding the publication of this manuscript.

adults (Clark et al., 2010) were used to co-excite multiple muscles in a musculoskeletal model. Each module was associated with specific biomechanical functions that resulted in a well-coordinated walking pattern. Module 1 (hip and knee extensors) contributed to body support in early stance while Module 2 (ankle plantarflexors) contributed to body support and forward propulsion in late stance. Module 3 (tibialis anterior and rectus femoris) decelerated the leg in early and late swing while generating energy to the trunk throughout swing while Module 4 (hamstrings) acted to absorb leg energy (i.e. decelerate it) in late swing while increasing leg energy in early stance to provide forward propulsion. Post-hoc analysis revealed a fifth module (Module 5: hip flexors) that accelerated the leg forward in pre- and early swing. However, since the model was constrained to the sagittal plane, the contributions of each module to mediolateral (ML) balance control and contralateral leg swing due to energy transfer through the pelvis could not be assessed.

Walking is a 3D movement in which non-sagittal plane biomechanical subtasks must be effectively executed. In addition to providing body support and forward propulsion, muscles must also control ML balance (Perry, 1967; Winter, 1995) by redirecting center-of-mass (COM) frontal plane movement. A recent 3D simulation analysis found the muscles that contribute significantly to body support and forward propulsion also regulate ML COM acceleration (Pandy et al., 2010). Furthermore, previous 3D walking simulations found that hip muscles in the ipsilateral leg are important for contralateral leg swing (Arnold et al., 2007; Hall et al., 2011; Peterson et al., 2010). Thus, it is unclear whether a similar simple modular control framework can capture 3D walking when muscles contributing to ML balance control and contralateral leg swing are considered.

The purpose of this study was to use a 3D musculoskeletal model and forward dynamics simulation of healthy walking to gain a comprehensive view of modular control of human walking. Specifically, we analyzed modular contributions to the 3D ground reaction forces (GRFs) and power generation, absorption and transfer among body segments. We hypothesized that: 1) a similar five module framework would be capable of driving a 3D model of walking; 2) modules important for body support and forward propulsion would also be important for ML balance (e.g., Modules 1 and 2); and 3) modules that include the hip muscles (e.g., Modules 1, 4 and 5) would play a prominent role in controlling contralateral leg swing.

Methods

Neuromuscular model

A previously described 3D musculoskeletal model (Peterson et al., 2010) with 23 degrees-of-freedom was developed using SIMM (Musculographics, Inc.) and included rigid segments representing the trunk, pelvis and two legs (thigh, shank, talus, calcaneus and toes). The pelvis had six degrees-of-freedom (3 translations, 3 rotations) with the trunk and hip joints modeled using spherical joints. The knee, ankle, subtalar and metatarsophalangeal joints were modeled as single degree-of-freedom revolute joints. The foot-ground contact forces were modeled with 31 independent visco-elastic elements attached to each foot (Neptune et al., 2000). Passive torques representing forces applied by ligaments, passive tissue and joint structures were applied at each joint (Anderson, 1999). The dynamical equations-of-motion were generated using SD/FAST (PTC).

The model was driven by 38 Hill-type musculotendon actuators per leg (five smaller foot muscles from Peterson et al. (2010) were excluded in our model due to their minimal contributions to the biomechanical subtasks). Five previously identified muscle activation modules (for details see Neptune et al., 2009) describing time-varying activation patterns relative to the gait cycle were used as the muscle excitation inputs (Fig. 1). Modules 1–4

were derived from experimentally collected EMG data (see *Experimental Data*). Muscles without recorded EMGs but with similar anatomical arrangement, biomechanical function and/or EMG activity were included in these modules. Muscles within each module received the same excitation pattern and timing, but the magnitude was allowed to vary between muscles. Muscles associated with Module 5 received a bimodal excitation pattern (Hall et al., 2011). The Other Muscles (Fig. 1) unassociated with a module also each received a bimodal excitation pattern, which allows the flexibility for two distinct peaks, one broader peak, or only one peak (while bimodal is allowed it might not be used). Muscle contraction dynamics were governed by Hill-type muscle properties (Zajac, 1989) and muscle activation dynamics were modeled using a non-linear first-order differential equation (Raasch et al., 1997). Polynomial equations were used to estimate musculotendon lengths and moment arms (Menegaldo et al., 2004).

Dynamic Optimization

A 3D walking simulation of a 120% of a gait cycle was generated using a simulated annealing algorithm (Goffe et al., 1994) that fine-tuned the muscle excitation patterns and initial joint velocities such that the difference between the simulated and experimentally measured walking data (see below) and muscle stress was minimized. Quantities included in the cost function were errors in the pelvis translations, trunk, pelvis, hip, knee and ankle joint angles and GRFs and muscle stress. Each bimodal excitation pattern had six optimization parameters (onset, offset and magnitude for the two modes) and each module pattern had two optimization parameters for timing (onset, offset) and a magnitude parameter for each muscle within the module. Initial parameter values were based on experimental data (joint velocities) and a previously optimized simulation (excitation parameters). To improve the tracking optimization convergence, tracking torques were applied at each joint to drive them towards desired experimental kinematics using proportional control (see Appendix A in the Web Supplementary Material). These torques were also included in the cost function in order to drive their magnitudes to zero.

Experimental Data

The experimental data used were a subset of the data in Clark et al. (2010). Kinematic, GRF and EMG data were collected from 14 healthy adults (63.1 ± 9.1 years; 2 male) as they walked for 30s at 1.2 m/s on an ADAL split-belt treadmill (Techmachine). All subjects provided informed consent prior to data collection. Using non-negative matrix factorization (Clark et al., 2010), modules were identified from EMG data collected using bipolar Ag-AgCL surface electrodes from the tibialis anterior, soleus, medial gastrocnemius, vastus medialis, rectus femoris, medial hamstrings, lateral hamstrings and gluteus medius of each leg using a telemetered EMG acquisition system (Konigsberg Instruments). 3D body-segment kinematics were collected at 100 Hz and GRF and EMG data were collected at 2000 Hz using Vicon Worksation v4.5 software. EMG signals were high-pass filtered with a fourth-order Butterworth filter (40 Hz), demeaned, rectified and low-pass filtered with a fourth-order Butterworth filter (4 Hz). The GRFs were filtered at 20 Hz. Kinematics were low-pass filtered with a fourth-order Butterworth filter with a cutoff frequency of 6 Hz. All EMG, GRF and kinematic data were time normalized to 100% of the gait cycle. Kinematic and GRF data were averaged across subjects for the simulation tracking.

Simulation Analyses

Analyses were performed on the last 100% of the simulation (a full gait cycle starting at heel-strike) to allow the initial transients to decay. To quantify contributions of each module to the biomechanical sub-tasks of body support (vertical GRF), forward propulsion (anterior-posterior, AP GRF), ML balance control (ML GRF) and ipsilateral and contralateral leg swing, individual muscle contributions to the GRFs and body segment

mechanical energetics were quantified using previously described GRF decomposition and body segment power analyses (Neptune et al., 2004). The contribution of each module to each sub-task was found by summing the individual muscle contributions from those muscles associated with that module. For RF, its contribution was scaled according to the relative contribution of the two modules (Fig. 1) to the muscle's total excitation.

Results

Using the five previously identified modules as excitation inputs (plus excitation of the remaining muscles, Fig. 1), the simulation emulated well the group averaged walking data with average kinematic and GRF deviations of 4.6° (experimental SD = 6.2°) and 4.3% body weight (BW, experimental SD = 2.9% BW), respectively (Fig. 2, Table 1). All tracking torques were eliminated except for small torques remaining for pelvis rotation (peak value of 3.9 Nm, average value of 0.3 Nm), which had minimal contributions to all walking subtasks. Module 1 (gluteus muscles, vasti and rectus femoris) provided body support (positive vertical GRF, Fig. 3b) and acted to decelerate the body (negative AP GRF, Fig. 3a) during the first half of stance and accelerated the body medially (positive ML GRF, Fig. 3c) throughout stance. Module 1 also transferred energy from the ipsilateral leg to the contralateral leg from early to mid-stance (Fig. 4). Module 2 (plantarflexors) provided body support throughout stance (Fig. 3b), decelerated the body during the first half of stance (Fig. 3a), and provided forward propulsion (positive AP GRF, Fig. 3a) while accelerating the body laterally (negative ML GRF, Fig. 3c) in the second half of stance. Module 3 (ankle dorsiflexors and rectus femoris) absorbed power from the ipsilateral leg during early stance and transferred that energy to the trunk (Fig. 4). Module 3 also helped control ipsilateral leg swing by accelerating the leg forward during swing (i.e. generated power to the leg). Module 4 (hamstrings) provided forward propulsion (Fig. 3a) and accelerated the body laterally during the first half of stance (Fig. 3c). Module 4 also delivered much energy to the ipsilateral leg in stance while delivering some energy to the contralateral leg prior to its swing through both power generation and power transfer from the trunk (Fig. 4). Finally, Module 4 also acted to decelerate the ipsilateral leg in late swing (Fig. 4). Module 5 (hip flexors) facilitated leg swing by generating positive power to the ipsilateral leg during swing (Fig. 4). Those muscles not associated with a module also contributed to walking subtasks (Figs. 3, 4). AM generated a lateral GRF in the first half of stance (Fig. 5a) while generating energy to the contralateral leg and trunk and absorbing energy from the ipsilateral leg (Fig. 5b). AL, AB and QF generated energy to the ipsilateral leg during early swing but decelerated the leg through energy transfer later in swing to assist the hamstrings (Fig. 5b). The hip abductors (GEM, PIRI, TFL) generated a medial GRF through mid-stance (Fig 5a) while transferring power from the contralateral leg to the ipsilateral leg and trunk (Fig. 5b).

Discussion

Recent evidence supports the idea that movements are controlled through a combination of co-excitation patterns, or modules, organized around specific biomechanical sub-tasks (e.g., Clark et al., 2010; d'Avella et al., 2003; Davis and Vaughan, 1993; Ivanenko et al., 2004; Neptune et al., 2009; Ting and Macpherson, 2005). For example, in kicking frogs, modules have been associated with controlling kick direction (d'Avella et al., 2003) and in standing cats, modules have been associated with different hind-limb force components (Ting and Macpherson, 2005). In human walking, modules have been temporally associated with particular regions of the gait cycle (Cappellini et al., 2006; Davis and Vaughan, 1993; Ivanenko et al., 2004), suggesting they provide specific biomechanical functions.

When a similar five module framework was used for 3D walking, the contributions of each module to forward propulsion and body support were consistent with our previous 2D

analysis (Neptune et al., 2009). Modules were also found to work synergistically throughout stance to control ML balance through their contributions to the ML GRFs. During most of stance the net GRF is directed medially (Fig. 3c), first acting to decelerate the laterally moving COM in order to maintain dynamic balance and prevent falling (e.g., prevent the COM from moving beyond the base of support) and then to help shift the body weight to the contralateral side in preparation for the next stance phase. This medial GRF is generated primarily by Module 1, which dominates the lateral contributions from the hip adductors (primarily AM, Fig. 5a) and Module 4 (Fig. 3c). The medial GRF from Module 1 is generated by the gluteus muscles (GMED, GMIN and GMAX), which dominate the small offsetting lateral contribution from VAS (Fig. 6). These opposing contributions of muscles within Module 1 are consistent with a previous simulation analysis that found similar opposing COM accelerations (Pandy et al., 2010). This co-activation is needed, however, for body support. Thus, more demanding ML tasks (e.g., turning) may reweight the relative muscle contributions within Module 1 to emphasize one of these opposing contributions to a greater degree (e.g., similar to the reweighting of Module 2 muscles that were found when body weight and mass were independently manipulated, McGowan et al., 2010). Near the end of stance, the direction of the net GRF switches from medial to lateral as Module 2's (plantarflexors) lateral contribution dominates the medial contributions by Module 1 and the hip abductor muscles (Fig. 3c, 5a). In support of our hypotheses, Modules 1 and 2 appear to be the primary modules contributing to ML balance control, which is consistent with a previous simulation analysis that found VAS, SOL, GAS, and GMED are the primary contributors to ML COM acceleration (Pandy et al., 2010). The hip ab/adductors, primarily AM in early stance, also play an important role in ML balance control, which suggests that the current five module framework is insufficient for 3D walking and that an additional neural control element may be needed to control hip ab/adduction.

In addition to controlling ipsilateral leg swing, modules also contributed to contralateral leg swing. In partial support of our hypothesis that modules containing the hip muscles would contribute to contralateral leg swing, Modules 1 and 4 generated energy to the contralateral leg (i.e. accelerated the leg into swing): Module 1 in early contralateral swing and Module 4 in contralateral pre-swing and swing (Figs. 4, 7). The magnitude of the power delivered by these modules to the contralateral leg is of similar magnitude as the power delivered to the ipsilateral leg by Module 5 during ipsilateral swing (Fig. 4), which highlights the important role Modules 1 and 4 have in controlling contralateral leg swing. While the energy transfer to the contralateral leg was not observed in Neptune et al. (2009), the present 3D model included additional degrees-of-freedom at the trunk, pelvis and hip, allowing for more energy transfer from the stance leg to the contralateral swing leg through pelvis rotation. These results are consistent with previous modeling studies that found power transfer to the contralateral leg from several of the muscles within these modules (e.g. GMED, GMIN, hamstrings) (Arnold et al., 2007; Hall et al., 2011; Peterson et al., 2010). These results are also consistent with previous studies deriving modules from bilateral EMG (Dominici et al., 2011; Olree and Vaughan, 1995). These studies identified a module active primarily around contralateral swing that includes several of the ipsilateral muscles that we include in our Modules 1 and 4 (e.g. GMED, VAS, TFL) and contralateral muscles that we include in our Module 5 (e.g. AL) that are important for leg swing. These results also provide support for the importance of bilateral coordination during walking.

The remaining muscles (Other Muscles), all hip ab/adductor muscles, were important for ML balance control (see above) and both ipsilateral and contralateral leg swing. Some hip adductors (AL, AB and QF) accelerated the ipsilateral leg forward during swing, similar to Module 5, and then decelerated the leg in late swing prior to heel-strike (Fig. 5b). The remaining hip adductor, AM, transferred energy from the ipsilateral leg to the contralateral leg prior to contralateral swing (Fig. 5b). One question that naturally arises is whether these

muscle contributions could be mapped into existing modules. To address this question, post-hoc analyses were performed in which the remaining muscles were placed into different modules. Simulations were generated with each of the remaining muscles placed into one of the original five modules rather than allowing them to be independently controlled. The hip abductors (GEM, PIRI and TFL) were placed into Module 1 due to the similarity in their optimized excitation patterns with Module 1. Similarly, AL, AB and QF were placed in Module 5 with the hip flexors due to their similarity in excitation timing to Module 5. The optimized excitation pattern for AM had similarities to both Module 1 and 4 patterns, therefore two simulations were generated with AM placed in either Module 1 or Module 4. Neither optimization eliminated the tracking torques while successfully reproducing the walking pattern. Thus, our hypothesis that a five module framework can successfully drive a 3D model was not supported.

The primary source of difficulty with using the five module framework was eliminating the hip ad/abduction tracking torques, which suggests that an additional module may be critical for non-sagittal hip motion control. Since AM was found to be a powerful contributor to ML balance control (Fig. 5a), another optimization was performed in which a sixth module was used to control all three components of AM. The optimization found that these six modules were able to successfully reproduce the 3D walking pattern with all tracking torques eliminated except for minimal torques for pelvis rotation (mean torque of 0.4 NM, mean joint angle error of 4.3°, experimental SD of 6.2°, and mean GRF error of 5.0% BW, experimental SD of 2.9% BW, Table 1). The biomechanical functions of Modules 1–5 remained the same while the new Module 6 (AM) generated a laterally directed GRF during early stance (Fig. 8a) and transferred energy from the ipsilateral leg to the contralateral leg prior to contralateral swing (Fig. 8b).

A potential limitation is that modules were derived from only 8 muscles per leg while the model was driven by 38 per leg. Remaining muscles were each placed into a module based on results from previous studies (see Appendix B in the Web Supplementary Material for details), however a number of muscles in our model have not been included in any previous experimental module study (with many of these being muscles that contribute to non-sagittal plane motion). Future research recording EMG from a larger dataset of muscles is needed to support our results. Given that we were unable to find an arrangement of all muscles into a five module framework, it seems likely that at least one additional module primarily composed of hip abductor or adductor activity exists. In addition, except for RF, each muscle was controlled using only one module even though each muscle is excited to some degree by each module (e.g., Clark et al., 2010). An area of future work will look at the effect of allowing each module to contribute to each muscle's excitation pattern. However, assuming that each muscle has been placed in its correct dominant module, the overall modular function should remain unchanged with only slight differences in the magnitude and timing.

In conclusion, while a five module framework can successfully simulate 2D walking (e.g. Neptune et al., 2009) it does not appear to provide the additional control needed for 3D walking. The results of this study suggest that a sixth module organized around the subtasks of ML balance control and contralateral leg swing can provide the additional non-sagittal plane control. The fact that the simulation emulated remarkably well the measured kinematics and GRFs using a reduced set of neural control elements provides further evidence that modular control strategies organized around task-specific biomechanical functions may be used to control complex human movements. Future work will be directed at understanding how execution of these biomechanical subtasks is altered in neurologically impaired populations due to impaired modular control.

Supplementary Material

Refer to Web version on PubMed Central for supplementary material.

Acknowledgments

The authors would like to thank Dr. Steve Kautz and Dr. Felix Zajac for their insightful comments on earlier drafts of the manuscript. This work was supported by NIH grant R01 HD468203 and the National Science Foundation Graduate Research Fellowship Program. The contents are solely the responsibility of the authors and do not necessarily represent the official views of the NIH or NINDS.

References

Anderson, FC. Doctoral Dissertation. The University of Texas; Austin, Austin, TX: 1999. A dynamic optimization solution for a complete cycle of normal gait.

Arnold AS, Thelen DG, Schwartz MH, Anderson FC, Delp SL. Muscular coordination of knee motion during the terminal-swing phase of normal gait. J Biomech. 2007; 40 (15):3314–24. [PubMed: 17572431]

Cappellini G, Ivanenko YP, Poppele RE, Lacquaniti F. Motor Patterns in Human Walking and Running. J Neurophysiol. 2006; 95 (6):3426–3437. [PubMed: 16554517]

Clark DJ, Ting LH, Zajac FE, Neptune RR, Kautz SA. Merging of Healthy Motor Modules Predicts Reduced Locomotor Performance and Muscle Coordination Complexity Post-Stroke. J Neurophysiol. 2010; 103 (2):844–857. [PubMed: 20007501]

d'Avella A, Saltiel P, Bizzi E. Combinations of muscle synergies in the construction of a natural motor behavior. Nat Neurosci. 2003; 6 (3):300–8. [PubMed: 12563264]

Davis BL, Vaughan CL. Phasic behavior of EMG signals during gait: Use of multivariate statistics. J Electromyogr Kines. 1993; 3 (1):51–60.

Dominici N, Ivanenko YP, Cappellini G, d'Avella A, Mondi V, Cicchese M, Fabiano A, Silei T, Di Paolo A, Giannini C, Poppele RE, Lacquaniti F. Locomotor primitives in newborn babies and their development. Science. 2011; 334 (6058):997–9. [PubMed: 22096202]

Goffe WL, Ferrier GD, Rogers J. Global optimization of statistical functions with simulated annealing. J Econometrics. 1994; 60 (1–2):65–99.

Hall AL, Peterson CL, Kautz SA, Neptune RR. Relationships between muscle contributions to walking subtasks and functional walking status in persons with post-stroke hemiparesis. Clin Biomech. 2011; 26(5):509–515.

Ivanenko YP, Poppele RE, Lacquaniti F. Five basic muscle activation patterns account for muscle activity during human locomotion. J Physiol. 2004; 556 (Pt 1):267–82. [PubMed: 14724214]

McGowan CP, Neptune RR, Clark DJ, Kautz SA. Modular control of human walking: Adaptations to altered mechanical demands. J Biomech. 2010; 43 (3):412–419. [PubMed: 19879583]

Menegaldo LL, de Toledo Fleury A, Weber HI. Moment arms and musculotendon lengths estimation for a three-dimensional lower-limb model. J Biomech. 2004; 37 (9):1447–1453. [PubMed: 15275854]

Neptune RR, Clark DJ, Kautz SA. Modular control of human walking: A simulation study. J Biomech. 2009; 42 (9):1282–1287. [PubMed: 19394023]

Neptune RR, Wright IC, Van Den Bogert AJ. A Method for Numerical Simulation of Single Limb Ground Contact Events: Application to Heel-Toe Running. Comput Methods Biomech Biomed Engin. 2000; 3 (4):321–334. [PubMed: 11264857]

Neptune RR, Zajac FE, Kautz SA. Muscle force redistributes segmental power for body progression during walking. Gait Posture. 2004; 19 (2):194–205. [PubMed: 15013508]

Olree KS, Vaughan CL. Fundamental patterns of bilateral muscle activity in human locomotion. Biol Cybern. 1995; 73 (5):409–14. [PubMed: 7578478]

Pandy MG, Lin YC, Kim HJ. Muscle coordination of mediolateral balance in normal walking. J Biomech. 2010; 43 (11):2055–64. [PubMed: 20451911]

Perry J. The mechanics of walking. A clinical interpretation. Phys Ther. 1967; 47 (9):778–801. [PubMed: 6051073]

Peterson CL, Hall AL, Kautz SA, Neptune RR. Pre-swing deficits in forward propulsion, swing initiation and power generation by individual muscles during hemiparetic walking. J Biomech. 2010; 43 (12):2348–2355. [PubMed: 20466377]

Raasch CC, Zajac FE, Ma B, Levine WS. Muscle coordination of maximum-speed pedaling. J Biomech. 1997; 30 (6):595–602. [PubMed: 9165393]

Ting LH, Macpherson JM. A limited set of muscle synergies for force control during a postural task. J Neurophysiol. 2005; 93 (1):609–13. [PubMed: 15342720]

Winter DA. Human balance and posture control during standing and walking. Gait Posture. 1995; 3 (4):193–214.

Zajac FE. Muscle and tendon: properties, models, scaling, and application to biomechanics and motor control. Crit Rev Biomed Eng. 1989; 17 (4):359–411. [PubMed: 2676342]

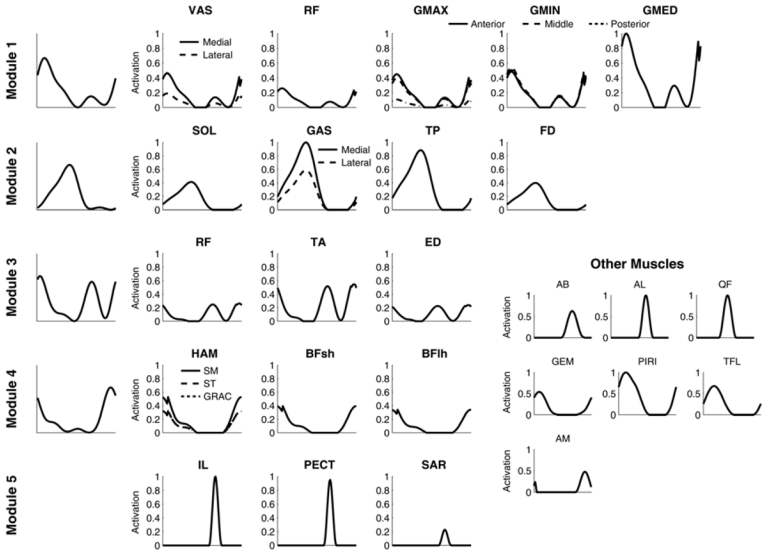

Figure 1.

Experimentally derived module patterns (left column, Modules 1–4) and the corresponding muscles excited by each module (rows). Module 1 included VAS (3-component vastus), RF (rectus femoris), GMAX (3-component gluteus maximus), GMIN (3-component gluteus minimus), and GMED (3 –component gluteus medius). Module 2 included SOL (soleus), GAS (medial and lateral gastrocnemius), TP (tibialis posterior), and FD (flexor digitorum longus). Module 3 included RF, TA (tibialis anterior), and ED (extensor digitorum longus). Module 4 included HAM (medial hamstrings = semimembranosus (SM) and semitendinosus (ST), gracilis (GRAC)), lateral hamstrings = biceps femoris long head (BFlh), and BFsh (biceps femoris short head)). Finally, Module 5 (Neptune et al. 2009) included IL (iliacus, psoas), PECT (pectinius) and SAR (sartorius). No experimental data were available for Module 5, thus a bimodal pattern was used. All muscles within a module received the same excitation timing and pattern, although the magnitude was allowed to vary. AM (3-component adductor magnus), AL (adductor longus), AB (adductor brevis), QF (quadratus femoris), GEM (gemellus), PIRI (piriformus) and TFL (tensor fascia lata), for which no experimental data were available, were not included in Modules 1–5 at first to allow them to have distinct anatomical and modular function. Thus, individual bimodal patterns were also used for these muscles.

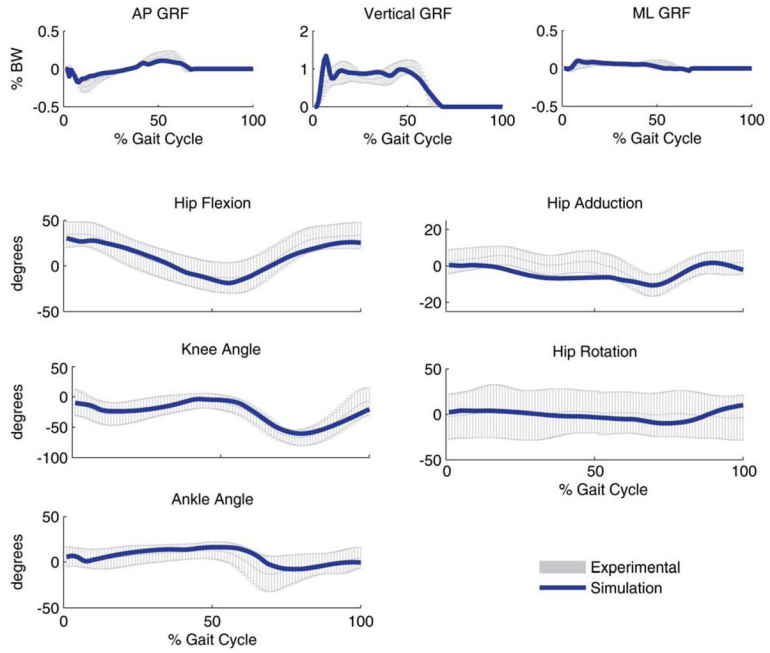

Figure 2.
Tracking results for the simulation controlled by five modules (plus excitation of remaining muscles). The simulated joint angles and ground reaction forces (blue lines) agree well with the experimental data (grey bars). The grey bars represent experimental means ± 2 SD.

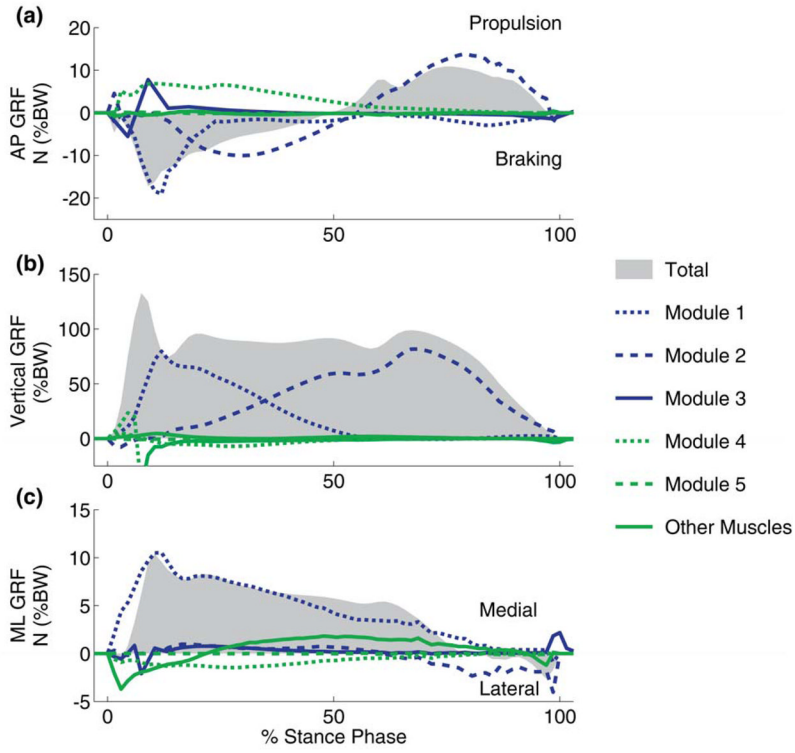

Figure 3.
Module contributions to the (a) anterior-posterior (AP), (b) vertical and (c) mediolateral (ML) ground reaction forces. Total is the sum of all muscles.

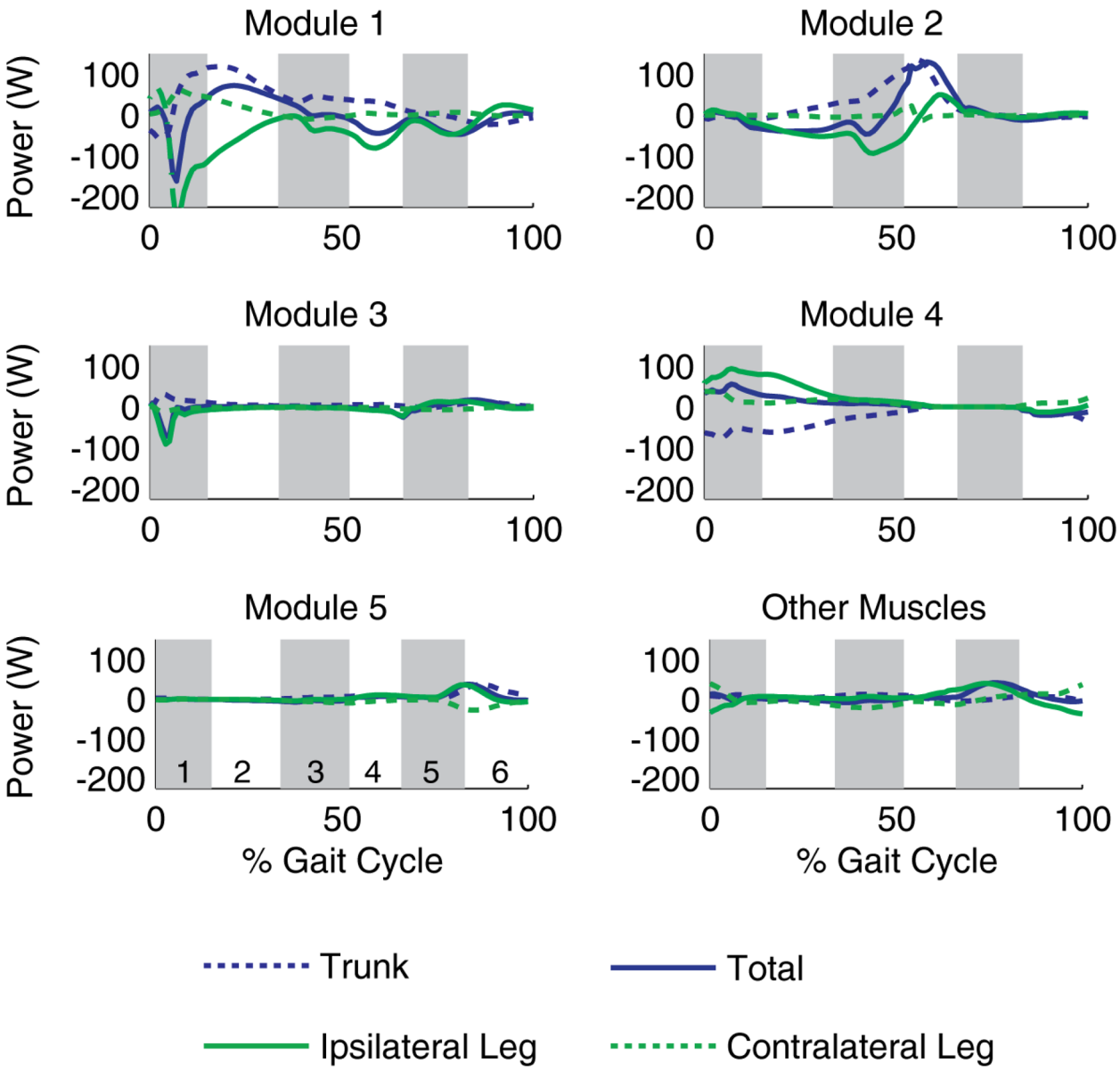

Figure 4.

Mechanical power delivered to the trunk, ipsilateral and contralateral leg by each module. Total represents the sum of the mechanical power delivered to all segments. Positive and negative power values indicate a module acts to accelerate or decelerate the segments, respectively. The alternating shaded regions represent different phases of the gait cycle: 1 – 1st double support/contralateral pre-swing, 2 – first half of ipsilateral single support/ contralateral swing, 3 – second half of ipsilateral single support/contralateral swing, 4 – ipsilateral pre-swing/contralateral 1st double support, 5 – first half of ipsilateral swing/ contralateral single support, and 6 – second half of ipsilateral swing/contralateral single support.

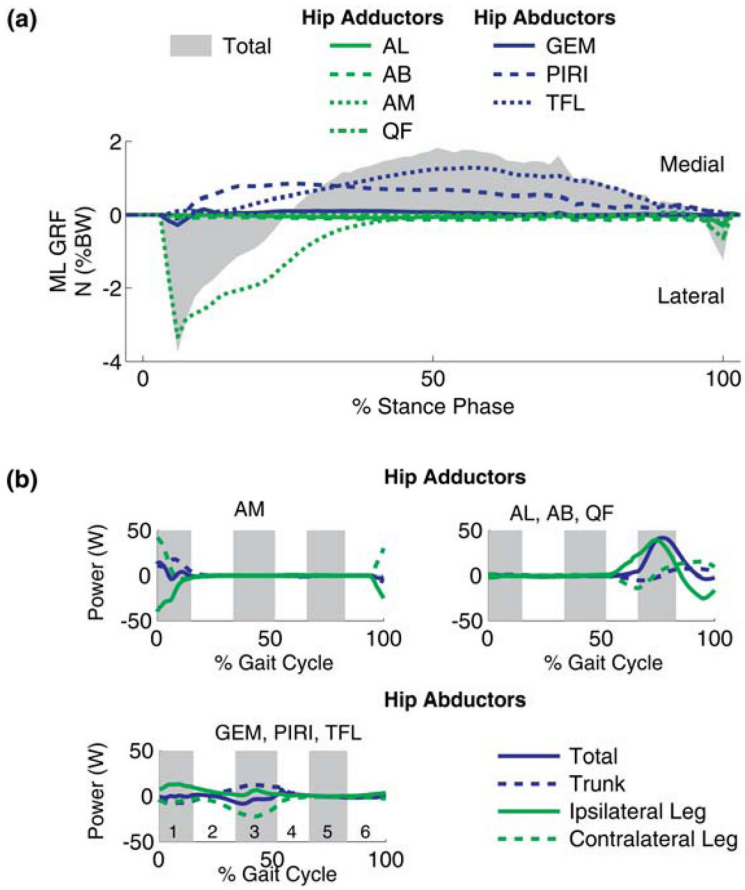

Figure 5.
Contributions from individual muscles not controlled by a module to (a) ML GRF and (b) power transfer among segments. The alternating shaded regions represent different phases of the gait cycle (see Fig. 3 caption).

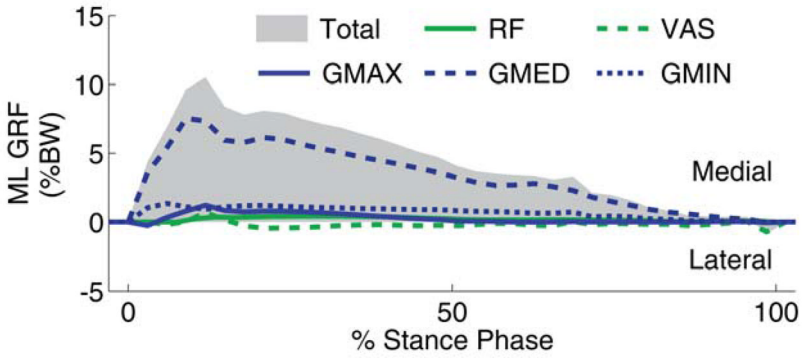

Figure 6.
ML GRF contributions from individual muscles in Module 1.

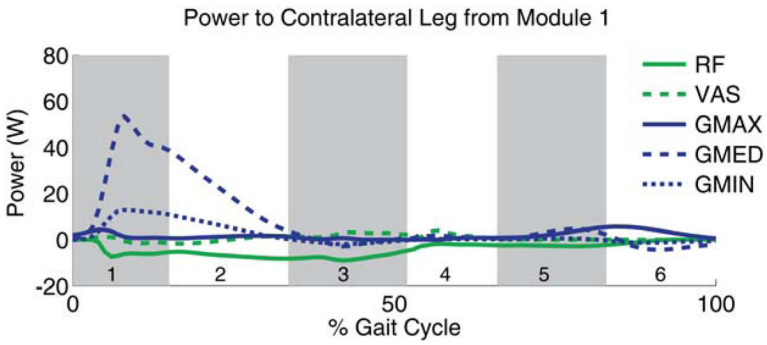

Figure 7.
Power delivered to the contralateral leg by Modules 1. The power transferred to the contralateral leg by Module 1 is primarily due to GMED and GMIN. The alternating shaded regions represent different phases of the gait cycle (see Fig. 3 caption).

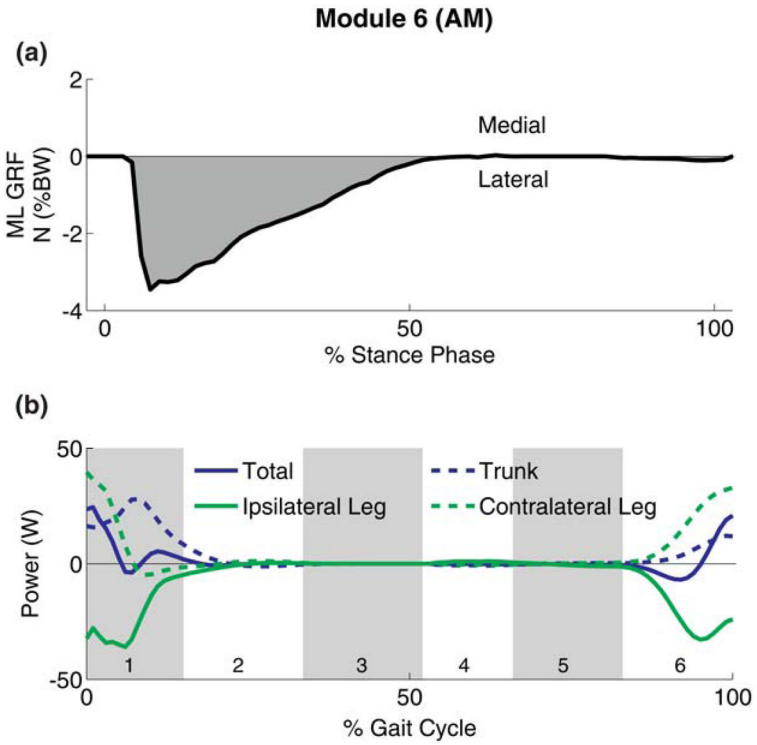

Figure 8.

Module 6 (AM) (a) generated a medial GRF during the beginning of stance and (b) decelerated the ipsilateral leg (negative power) during late swing and early stance while generating energy to the contralateral leg and trunk (positive power). The alternating shaded regions represent different phases of the gait cycle (see Fig. 3 caption).

Table 1

The average difference between the experimental and simulated kinematic angles and GRFs compared to the average standard deviation (SD) of the experimental data for the original five module simulation and the final six module simulation.

			5 Modules	6 Modules	SD
Kinematic Angles (°)	Pelvis	Obliquity	4.1	4.7	3.6
		Rotation	5.0	3.7	6.0
		Tilt	1.6	1.5	10.1
	Trunk	Obliquity	3.4	3.3	6.0
		Rotation	4.4	4.5	13.2
		Tilt	1.6	1.8	12.0
	Ipsilateral leg	Hip adduction	5.6	4.6	8.4
		Hip rotation	5.4	3.0	32.0
		Hip flexion	5.5	4.6	11.8
		Knee flexion	8.5	7.5	11.9
		Ankle angle	6.2	5.4	8.2
	Contralateral leg	Hip adduction	4.2	5.2	5.8
		Hip rotation	5.3	3.2	25.0
		Hip flexion	4.8	5.2	15.1
		Knee flexion	4.7	5.9	16.2
		Ankle angle	4.0	3.9	11.9
Forces (%BW)	Ipsilateral leg	AP GRF	3.3	4.1	2.8
		Vertical GRF	8.2	10.3	12.3
		ML GRF	2.2	2.0	1.9
	Contralateral leg	AP GRF	2.8	2.9	3.1
		Vertical GRF	7.9	8.8	12.8
		ML GRF	1.6	1.8	2.0
Average Angle Difference (°)			**4.6**	**4.3**	**12.3**
Average GRF Differences (%BW)			**4.3**	**5.0**	**5.8**